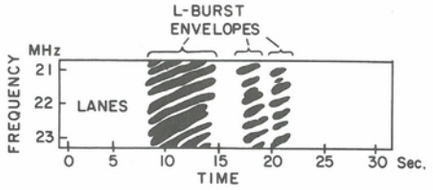

Fig. 7.11. An idealized sketch illustrating *L*-burst envelopes caused by interplanetary scintillations and drifting modulation lanes as they would appear in a dynamic spectrum. Adapted from Riihimaa [1971].

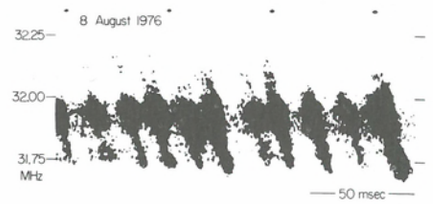

Fig. 7.12. A dynamic spectrum showing a train of simple *S* bursts recorded near 32 MHz by Desch, Flagg, and May [1978]. Notice that the full display covers a time interval of less than 200 ms, with an effective frequency and time resolution of 3 kHz and 0.3 ms, respectively.

At time resolutions shorter than about 0.01 s, *S* (short) bursts become apparent. These short-lived and rapidly drifting emission features are shown in Figure 7.12. The *S*-burst modulation is also a source-related phenomenon, appearing only in association with Io-stimulated emission. They will be discussed in detail.

Any or all of the above phenomenology is observable during an active period. Thus, a given storm always consists of spectral arcs of one variety or another but the nature and even occurrence of *S* bursts and modulation lanes depend on the CML, Io phase and observing frequency.

On much longer timescales, years for example, variations in activity become apparent following statistical analysis of the data. The best known of these is the 11.9-yr modulation, corresponding approximately to the length of a Jovian year. This modulation [Carr et al., 1970] has been shown to correlate best with the Jovicentric declination of the observer (D_E for an Earth-based observer), indicating that the radiation is strongly beamed latitudinally. Striking evidence for this (see, e.g., Fig. 7.13) is the almost complete disappearance of DAM at some frequencies during Jovian apparitions for which D_E is near its most negative value ($-3.3°$).

Finally, there are more subtle variations in the activity level, which appear on a scale of days to weeks. These are partially geometrical; that is, they are due to changes in the CML and Io phase required to observe storms associated with particular source regions. However, some of these variations are possibly due to some form of solar influence, such as to fluctuations in the solar-wind pressure and/or interplanetary magnetic field orientation across the Jovian magnetosphere. The latest and most sophisticated work on this problem has been done by Terasawa, Maezawa, and Machida [1978], Barrow [1979], and Levitskii and Vladimirski [1979]. All of these authors have found solar influences effective in modulating DAM; the solar variable examined ranged from sector boundary and stream–stream interactions in the solar wind to the geomagnetic A_p index. These studies indicate that decametric activity can be enhanced in direct response to a disturbance propagating with the solar wind. It should be understood, however, that these studies pose a complicated analysis problem involving the complete removal of the Io-controlled (geometry-related) events and the necessity of working with incomplete data sets. The arguments are necessarily statistical and there is not yet general agreement as to the nature and, indeed, even the existence of a solar influence. Not yet examined is the possibility that Io vulcanism has some influence on these variations.

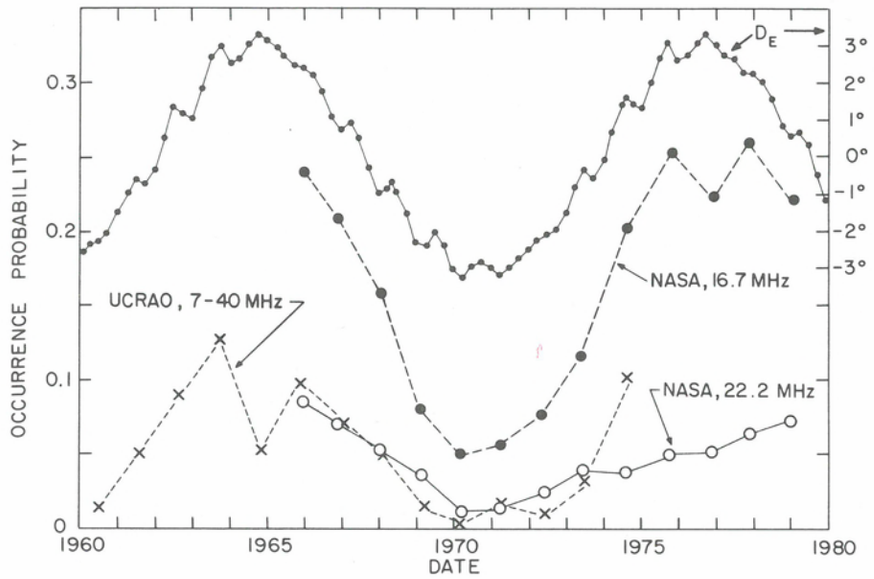

Fig. 7.13. A plot of the apparition-averaged probability of occurrence of DAM (three lower curves) and the jovicentric declination of the Earth, D_E, from 1960 to 1980. The x's correspond to swept-frequency measurements of DAM between 7 and 40 MHz obtained at the University of Colorado Radio Astronomy Observatory [Warwick et al., 1975], and the large circles and dots pertain to fixed-frequency measurements obtained with the NASA multistation Jupiter Monitor Network. Notice that the long-term variations in DAM activity correlate well with D_E in spite of the fact that D_E varies only by $\pm 3.3°$.

CML and Io phase control. The distribution of Jovian storms in time represents a well-organized, nonstochastic process. This is manifestly evident when active periods are superposed in histogram form using starting epochs separated by about 10 h. An example is shown in Figure 7.14, which shows results at 18–22 MHz [Thieman, 1977]. A three-peaked distribution is generally seen above about 10 MHz. Each individual peak in the DAM range has come to be called a radio "source" with varying nomenclatures (see Table 7.4). The sources can be maintained at the same longitude over long periods of time by choosing the proper interval between epochs [Carr, 1972b]. Such efforts have led to very accurate determinations of the rotation period of Jupiter's magnetic field and to the establishment of a strict upper limit of < 0.03 s/yr on possible linear secular changes in that period (see, e.g., May, Carr, and Desch [1979]). The latter determination indicates that Jupiter's rotation is very stable over a timescale of at least a decade. Other methods of determining Jupiter's rotation period have also been employed successfully. Duncan [1971] used a two-dimensional periodogram analysis, solving for Jupiter's period by sorting in both CML and Io phase space. Kaiser and Alexander [1972] used the method of power spectral analysis. These measurements of DAM and other period determinations at DIM wavelengths (e.g., Berge [1974]) led to the official adoption of a radio longitude system, called System III (epoch 1965). This system is based on a rotation rate of 870.536 deg/day (9 hr 55 min 29.71 s) [Riddle and Warwick, 1976; Seidelman and Divine, 1977]. It is used universally for specifying both the central meridian longitude, or CML (1965), and the longitude of meridians which corotate with the planet (see discussion of decimetric rotation period measurements in Sec 7.2).

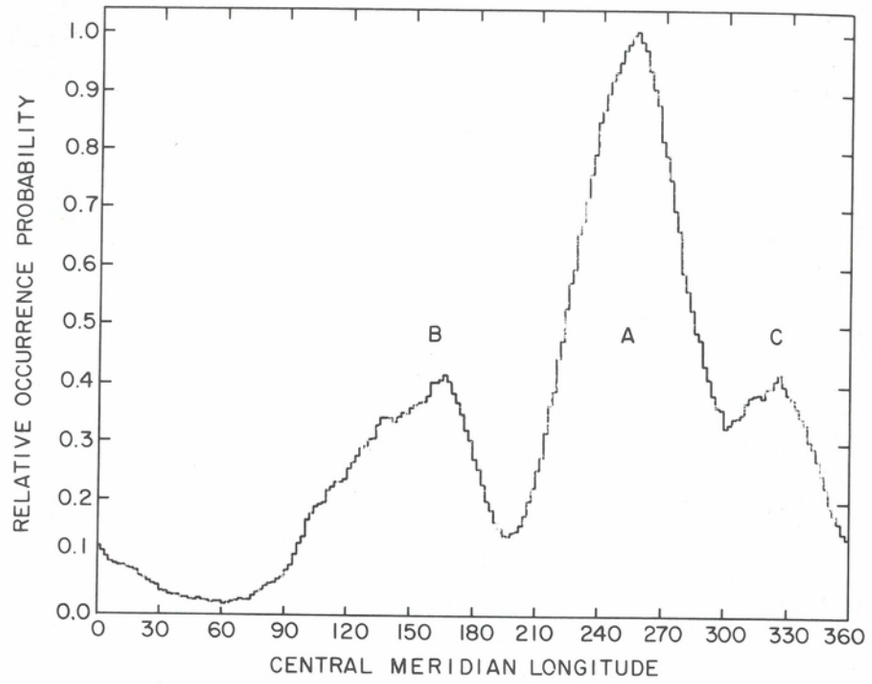

Fig. 7.14. Variation of the relative probability of occurrence of DAM as a function of central meridian longitude. The data were compiled by Thieman [1977] from observations at 18, 20, and 22 MHz carried out between 1957 and 1975 at the University of Florida and University of Texas radio observatories.

If we take the same data used to make Figure 7.14 but replot the events as a function of two variables, CML and Io phase, we obtain a plot like that shown in Figure 7.15. Here Io phase is plotted, as usual, in terms of angular departure from superior conjunction relative to the observer. This figure illustrates several important morphological features of DAM, most notable among them the control of the radiation by Io. Io modulation of DAM is not a subtle effect. Note that the B source, $80° < \text{CML} < 200°$, is observed only infrequently, except when $80° < \gamma_I < 110°$. When Io is in the preferred location, centered at about 90° γ_I, the emission "turns on," increasing flux levels a hundredfold over average source B intensity levels [Desch, Carr, and Levy, 1975; Desch, 1980]. We refer to the intense component as the Io-related source B, or just Io-B, and to the remainder of the emission as the non-Io-B source. Similar remarks apply to sources A and C, except that the preferred Io phase is centered on 240° γ_I. Source D seems to have only an Io-dependent component, which is shifted in Io phase relative to Io-B. The preferred Io phase for source D is about 105° γ_I.

Each of these principal sources has a characteristic frequency-time dynamic spectrum that is illustrated schematically in the smaller panels in this figure. The detailed behavior of the frequency ranges, arc shapes, and nose frequencies will be described.

At frequencies below about 10–15 MHz the CML-γ_I morphology is different from that just described. In the 5-MHz-wide band centered on the 10 MHz spectral peak, the emission is more continuous as a function of CML than it is at higher frequencies. This emission is made up principally of lesser arcs as mentioned previously. Below 2 MHz, the HOM once again exhibits strong CML modulation as suggested by the polarization

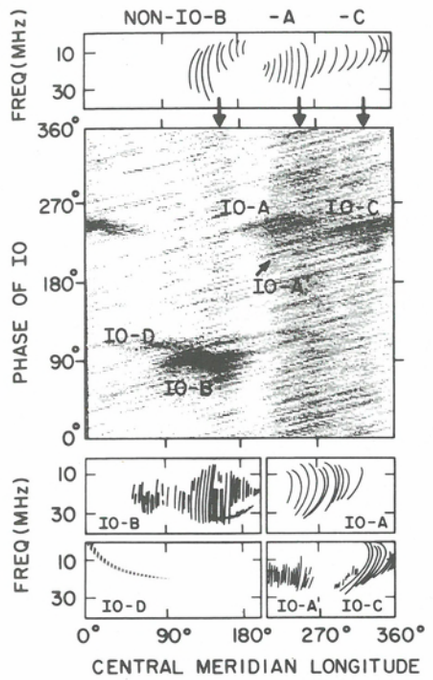

Fig. 7.15. Two-dimensional dependence of DAM activity on longitude (CML) and Io phase (γ_I) at about 20 MHz (J. R. Thieman, personal communication). The Io-related sources are each labeled in the CML-Io phase plot and schematic illustrations of the Io-dependent dynamic spectra are shown in the four lower panels. The top panel illustrates the dynamic spectral behavior of the Io-independent emissions. See text for details.

plot in Figure 7.17. In this frequency band HOM is rarely seen in the CML range 150° to 250°, that is, when the longitude meridian containing Jupiter's north magnetic dipole tip is facing, or nearly facing, the spacecraft. At still lower frequencies the kilometric-wavelength emission is evident and will be discussed separately later.

Polarization. It has long been known that the polarization sense of radiation from sources A and B (the principal ones at the higher frequencies) is predominantly right hand (RH), but as the frequency is decreased below about 20 MHz, progressively more left hand (LH) polarization becomes apparent outside the A–B longitude region (see Carr and Desch [1976], and references therein; see footnote in Section 7.2 of this chapter for definition of LH and RH polarization senses). It was recognized that these observations are consistent with the tilted-dipole field model if it is assumed that emission is in the extraordinary mode, and that the sources are relatively close to the planet. The evidence for this is that most RH polarization occurs within approximately $\pm 90°$ of the CML toward which the northern-hemisphere end of the magnetic dipole is tipped (200° λ_{III}) and that most LH occurrences are within the other 180° of CML. This implies that the magnetic dipole moment is approximately parallel rather than antiparallel to the rotation vector; that is, that the field lines emerge from the northern Jovigraphic hemisphere, as was later verified by DIM observations and Pioneer magnetometer measurements. The polarization senses of DAM and of the circular component of DIM are usually opposite; the reason for this, on the basis of the above model, is clear from Figure 7.8*b*.

These general conclusions regarding the polarization sense of DAM were based on fixed-frequency observations made at a relatively few select frequencies. The Voyager radio astronomy measurements of polarization sense extend over the entire frequency band of the Jovian emission, however, and we illustrate some of these observations in Figure 7.16. The polarization sense during four consecutive rotations is shown in the

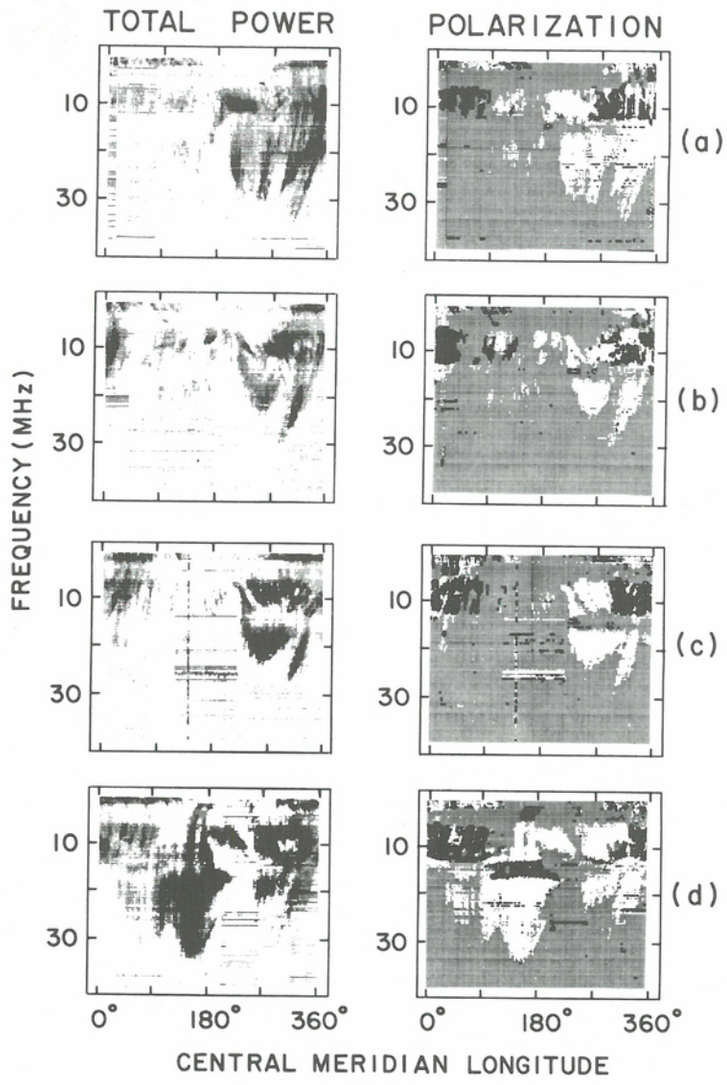

Fig. 7.16. Dynamic-spectral displays of the total received power (left-hand panels) and sense of polarization (right-hand panels) of DAM observed by Voyager 2 during four successive rotations of Jupiter. The top panels begin at 2330 spacecraft event time on July 2, 1979 and the bottom panels end 40 hours later at 1518 on July 4, 1979. The polarization display is coded so that right-hand polarized emission is white, left-hand emission is black, and intervals with no emission or unpolarized emission are grey. The Voyager antenna and impedance patterns produce bands of low sensitivity centered near 5 and 15 MHz, and occasionally the indicated polarization is artifically reversed. This effect can be seen in panel (*d*) between longitudes of about 100° and 210° where the polarization appears to be left-hand in spite of the overwhelming presence of right-hand emission at surrounding frequencies. The high frequency event at high longitudes in panel (*a*) is an Io-C storm, and the event centered near 150° in panel (*d*) is an Io-B storm. Notice the pattern of left-hand emission below 90° and above 270° at frequencies near 10 MHz. Note also the predominance of right-hand polarization at all longitudes for frequencies above 15 MHz.

right-side panels with the convention that white is RH polarized, black is LH polarized, and gray is unpolarized or no emission. Note the predominance of RH (white) polarization for each storm at all frequencies above about 12 to 14 MHz. Exceptions to this rule (not shown here) are the Io-D source, which is often LH and Io-C source, which can be LH polarized up to 20 MHz but rarely so at higher frequencies.

Three parameters are needed to specify the polarization state of a wave if total intensity is selected as the fourth (see Sec. 7.2 for a discussion of polarization parameters). The three most often used in DAM polarization measurements are (1) the axial ratio, with sign to indicate left-hand or right-hand sense, (2) the tilt angle of the major axis of the polarization ellipse, and (3) the degree of polarization, that is, the ratio of the polarized to the sum of the polarized and unpolarized power. Because of the effect of terrestrial ionospheric instability, in only one paper [Parker, Dulk, and Warwick, 1969] have ground-based measurements of the tilt angle been considered reliable. The degree of polarization was found by Barrow and Morrow [1968] to be > 0.70 for about 80% of the time at 18 MHz. Similar results were obtained at other frequencies (e.g., Sherril [1965]), and the generalization is usually made that the Jovian emission is nearly completely polarized across its entire frequency range. Measurements of the axial ratio r have indicated that DAM is elliptically polarized with $1 < r < \infty$ at the higher frequencies, becoming more nearly circular ($r = 1$) toward 10 MHz [Kennedy, 1969].

Because the only unambiguous polarization information provided by the Voyager radio astronomy receiver is the polarization sense, that is, whether the RH or LH circular component is the larger, we must continue to rely on the earlier fixed-frequency ground-based measurements. Between 5 and 15 MHz, where the lesser arcs are often almost continuous, agreement between Voyager and earlier ground-based [Dowden, 1963; Kennedy, 1969] polarization sense measurements appears to be good. LH polarization is observed from 0° to 135° CML, RH polarization from 135° to 300° CML. Between 300° and 360°, both senses are observed.

Polarization measurements below 2 MHz have been made only by the Voyager radio astronomy experiment. In Figure 7.17 we show 10 rotations of the planet with the time for 0° CML indicated in each rotation. The hectometric (HOM) emission is the black and white striped activity centered on 0° CML. The emission at the lowest frequencies, centered at about 200° CML, is kilometric emission (KOM), to be discussed later. The HOM displays fairly clear polarization reversals as a function of CML. For example in Figure 7.17, RH (white) polarization is generally evident between 0° and 90° CML where it is flanked by LH (black) emission centered at 330° and 100° CML. The LH polarization is apparently of greater absolute intensity because relatively far from the planet the RH component is below the receiver detection threshold and only the LH polarized emission was detected [Kaiser et al., 1979].

Although the DAM polarization pattern remains unchanged as viewed on the Voyager outbound trajectory (relative to inbound), the polarization pattern below 1 MHz is not as clearly defined outbound as it is inbound. Some limited CML ranges, for example the early longitude RH band, may even have reversed polarization (see Alexander et al. [1981] for details). Additional work is needed to clarify this phenomenon.

Detailed properties

Dynamic spectral landmarks. One of the most distinctive characteristics of the DAM concerns the repeatability of both coarse and fine emission features within the dynamic spectra. As first discussed by Warwick [1964] and Dulk [1965], both the Io-dependent and Io-independent emission sources have unique morphologies in

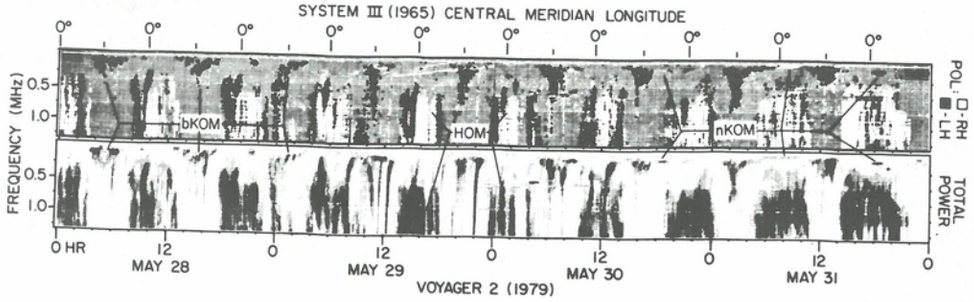

Fig. 7.17. Dynamic-spectral plots showing the polarization (upper panel) and total intensity of HOM and KOM (kilometer-wavelength emission) for ten consecutive rotations of Jupiter. Polarization sense is coded such that RH is white and LH is black. Episodes of HOM recur at 10-hr intervals centered near 0° central meridian longitude and tend to show both right- and left-hand polarization in a left-right-left (black-white-black) sequence. Left-hand polarized bKOM (broadband KOM) can be seen centered at about 200° CML in between each HOM episode.

frequency-time spectra that repeat on a rotation-by-rotation basis or, in the case of the Io-dependent sources, when the same CML and Io phase coordinates are presented to the observer. It is the latter dependence that is particularly striking. Furthermore, the features are apparently so stable over very long periods of time that comparison of landmark events separated by a Jovian year (~ 11.9 yr) may be used to measure the Jovian rotation period with considerable precision [Alexander, 1975].

This "permanent" spectrum, as it is called, is apparent on two timescales. On a scale of tens of minutes to hours, each source has a characteristic emission envelope, defined by its upper and lower frequency limits vs. time. And on a timescale of minutes, the spectral arcs, which form a kind of skeleton within each source, have a characteristic curvature, repetition rate, and vertex frequency (i.e., the frequency at which a vertical line is tangent to a given arc). The envelope landmarks were first described by Warwick [1964] and Dulk [1965] from ground-based studies. Using the notation of Table 7.4, Io-B is the most broadbanded of the sources and, as viewed from Earth, extends from frequencies below the ionospheric cut-off up to the magnetic cut-off at 39.5 MHz. In the best-developed cases the early phase of Io-B storms exhibits a drift of the high-frequency envelope from lower to higher frequencies, followed by a long, narrow-band tail that drifts down in frequency. The fabled high-frequency cut-off can be reached either during the development of the upward drifting envelope or by the narrow-band tail which follows it. The Voyager-PRA records (see Fig. 7.15) show that Io-B is made up of vertex-early arcs, closely spaced, with large radii of curvature – that is, they almost "stand up." When the CML-Io phase geometry is appropriate for Io-B (150° CML, 90° γ_I), the arcs can extend from about 1 MHz up to 39.5 MHz. For a given range of CML, the emission features evolve in a systematic fashion as the Io phase progresses from 60° to 120° [Dulk, 1965; Boischot et al., 1981].

The Io-A source is nearly the mirror image of Io-B. The sample spectrum in Figure 7.18 shows how the upper-frequency envelope drifts up and then down in frequency with time, like Io-B, but the spectral arcs are oriented vertex late. Generally, the Io-A arcs have smaller radii of curvature with lower vertex frequencies than those of Io-B, and they generally do not extend quite as high in frequency. Vertex frequencies are in the range of 10 to 12 MHz.

In addition to the traditional Io-A source, observed for $230° < \gamma_I < 250°$, Leblanc [1981] has noted that an additional Io-related-A (Io-A′) emission extends to slightly

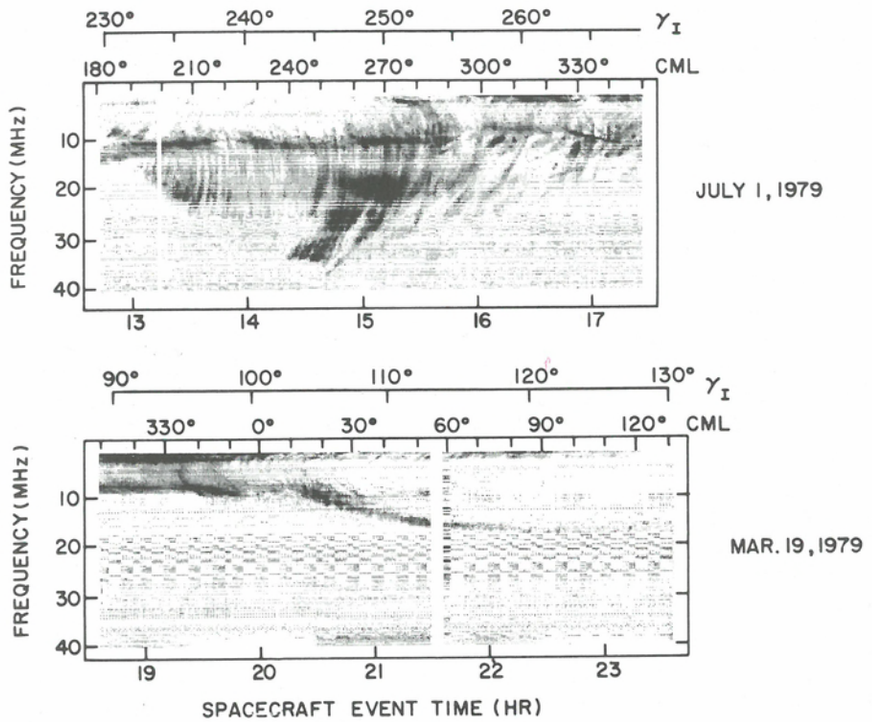

Fig. 7.18. Typical dynamic spectra of Io-A (upper panel) and Io-D (lower panel) events from Voyager Planetary Radio Astronomy experiment.

lower Io phase. The identification is based on characteristic spectral forms which, like Io-A, are vertex late arcs but with very little curvature and very compressed frequency range. This emission rarely extends below 10 MHz or above 25 MHz.

The Io-C source (at CML > 270°) in Figure 7.16*a* displays a characteristic negatively drifting envelope made up of vertex late arcs with small curvature. Vertex frequencies are commonly near 10–15 MHz or below. The upper-frequency limit of the Io-C source is only rarely greater than 30–32 MHz.

The Io-D source generally corresponds to only one slowly drifting narrow band of emission. The event shown in Figure 7.18, for example, drifts slowly up in frequency from about 5 MHz to 18 MHz over a period of slightly over 2 h. This source often has the appearance of a single, long, vertex-early arc, but it may actually consist of finely structured sections of arcs. The vertex frequency, when visible, is always below 10 MHz.

The Io-independent A- and B-source spectra often appear as less well-developed versions of the Io-dependent components. The intensities are much smaller, the frequency range of the arcs appears somewhat compressed, and the curvature is greater, that is, the Io-independent arcs are not as nearly vertical as the Io-related arcs. The restricted frequency range is probably an intensity threshold effect, however, as originally suggested by ground-based observations [Desch et al., 1975] and confirmed by recent Voyager observations [Barrow and Desch, 1980; Barrow and Alexander, 1980]. The high frequency limit of non-Io-B, for example, is at least 36 to 38 MHz; of non-Io-A, 32 to 34 MHz; and of non-Io-C, 30 to 32 MHz. The values are not much less than

the Io-related source high-frequency cut-offs. The strong implication here is that, if emission is at or near the local electron cyclotron frequency, then stably trapped particles alone cannot account for either the Io or non-Io radiation because the maximum magnetic field strengths in the southern hemisphere are not high enough to support these peak frequencies. That is, the conjugate mirror points at these relatively high frequencies in the southern hemisphere would be below the ionosphere.

All of the traditional sources described up to now have consisted of greater-arc emission. However, often superposed on the greater arcs in the 2 to 20 MHz band are intense lesser-arc emissions, so called for their restricted frequency range. Some of this emission is evident in Figure 7.10. Lesser-arc emission appears more nearly continuous compared to the episodic occurrence of the greater-arc events. This radiation is independent of Io control.

Below about 2 MHz, the spectra seem more amorphous than at higher frequencies. There is some evidence that most, if not all, of this radition is simply the lower-frequency extension of the DAM greater and/or lesser arcs.

All of the DAM arcs seem to share certain statistical properties. For example, the average single-frequency duration and time interval between arcs is 3 to 6 min; however, the arcs are not periodic in time. The depth of modulation between arcs can be 20 dB (factor of 100 in power) or greater. The arc vertex frequencies seem to vary in a systematic way as a function of CML. Staelin [1981] has related this variation to the O_4 magnetic field model [Acuña and Ness, 1976c] in the context of a conical beam pattern.

Local time effects. We noted earlier with regard to Io control of DAM that Io phase is almost always plotted relative to the observer rather than, say, the Sun. Early ground-based studies showed that the Io effect is most pronounced in geocentric as opposed to heliocentric coordinates, implying that the observed morphology is due to the passage of a narrowly filled radiation cone past the observer [Bigg, 1964; Dulk, 1967]. According to this view, the preferred coordinates should remain at 90° and 240° γ_1, even in the event of large changes in the observer's local time relative to Jupiter. (Local time is defined here as the Sun–Jupiter–observer angle, measured in degrees or hours, where 12 h corresponds to 0° local time.) As viewed from Earth, the Sun–Jupiter–observer angle varies only between ±12°, so a definitive test of this model could not be made until Voyager was on its outbound flight path after Jupiter encounter. The results are shown in Figure 7.19. Here the preencounter and post-encounter morphologies as observed from Voyager 1 and Voyager 2 are compared at 20 MHz, and it is evident that the concept of radiation beams rotating with the planet is substantiated [Alexander et al., 1981]. The local times are about 10 and 4 hr, respectively, corresponding to an angular change of about 90° between the two observing geometries. The Io-controlled sources B, A, and C are clear in both panels and their preferred Io phase and CML locations are unchanged to within the effective grid size of the plots. Alexander et al. also stressed that the occurrence probability levels did not appear to change after encounter, both were consistent with 100% probability of detection. Also as expected from the corotating beam model, the polarization sense of the sources did not change after encounter.

On the other hand, Alexander et al. show that the non-Io emission undergoes a dramatic change in occurrence probability level between pre- and post-encounter observing intervals, in contrast to the Io-related emission (see Fig. 7.19). Note that the non- Io-B events (CML < 200°) become much more common after both the Voyager 1 and Voyager 2 encounters, whereas the non-Io-A events (CML > 200°) are greatly enhanced before encounter. Examination of the source flux density levels indicates

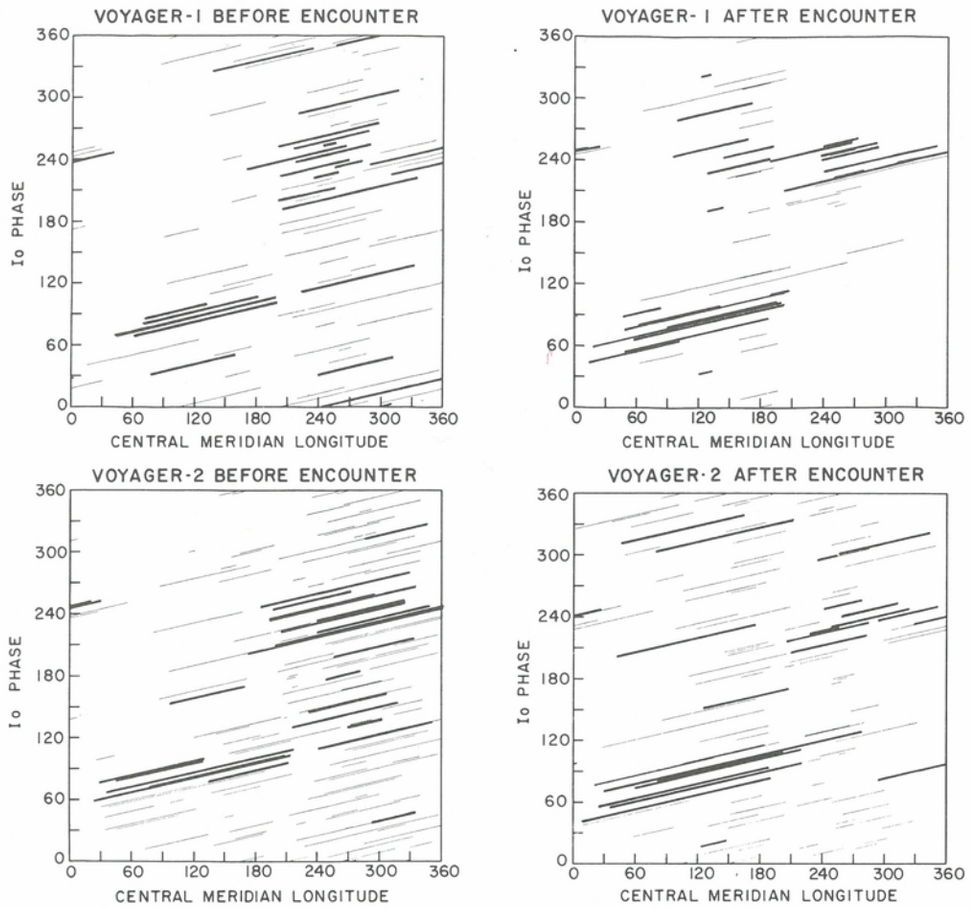

Fig. 7.19. Plots of the occurrence of DAM at frequencies above 20 MHz observed by Voyager 1 (above) and Voyager 2 (below) for one-month intervals before (left) and after (right) encounter as a function of CML and Io phase (γ_1). The heavy lines denote those events that extended to 30 MHz or higher, and so they tend to concentrate in regions of the diagram associated with Io-related activity. After encounter there is a shift in the preferred longitude for Io-independent DAM but no change in Io-related DAM. From Alexander et al. [1981].

that these changes may primarily be a consequence of changes in emission intensity, rather than of the total absence of one component. In basing non-Io source A and B identifications on dynamic spectral properties, that is, vertex-late vs. vertex-early are curvature, respectively, Leblanc [1981] independently came to the same conclusions as Alexander et al. regarding the intensity changes of the two sources after encounter.

Below 15 MHz and above 1 MHz the lesser arc emission is dominant, and here there is also evidence of a local time effect in the data [Alexander et al., 1981; Leblanc, 1981]. The occurrence probability of emission at longitudes below about 140° decreases after encounter, and the lesser arcs with vertex-late curvature become weaker and rare.

The important question arises as to how the local time effect is caused by the Sun. Two types of solar influence that could conceivably produce such an effect are solar photons and the solar wind. If it is the latter, the local time effect might be expected to

depend on the solar wind activity level in some observable way. But if solar photons are responsible, the effect may be due somehow to the ionizing action of ultraviolet radiation in the ionosphere. If so, new clues to the emission or initial propagation of DAM will be at hand. In any event, the recent discoveries of the Jovian local time effect and the dynamic spectral arcs are providing new impetus to the search for the origins of DAM.

S bursts. The Jovian *S* bursts, or millisecond bursts as they are sometimes called, were first recognized by Gallet [1961] who noted a clear distinction between *L*- (long) bursts and *S*-(short) bursts, a distinction that is still made today. The fundamental differences between the two types of emission were pointed out earlier: the *L*-burst modulation envelope originates largely in the solar wind and has a timescale of a few seconds; the *S*-burst modulation is intrinsic to the source or to its immediate surroundings and has a timescale of milliseconds. Although the *S* bursts account for a relatively small fraction of the DAM emission – probably less than 10% – their source-intrinsic nature makes them of such interest that they have undergone intense scrutiny since their discovery.

A sample *S*-burst dynamic spectrum is shown in Figure 7.12. (Readers wishing to examine many more *S* bursts are referred to an atlas of spectra by Ellis [1979]). These are so-called simple *S* bursts whose phenomenology is easily described: they usually have narrow (< 200 kHz) instantaneous bandwidths, single-frequency durations of 10 to 100 ms, and rapid frequency drift rates (df/dt) ranging from -5 to -45 MHz/s. It is important to note that the drift rates are always negative; that is, simple *S* bursts invariably drift from higher to lower frequencies with time. The total band through which the bursts drift is generally less than a few MHz, which explains why Gallet [1961] never saw bursts simultaneously on his two channels, which were separated by 2 MHz. A further important characteristic of the *S* bursts is their strict association with Io-dependent emission sources and, in fact, with only certain CML and Io-phase values within a given Io-related source [Riihimaa, Dulk, and Warwick, 1970; Leblanc and Genova, 1981]. More complex *S* bursts, which nearly defy classification, have also been described in the literature (see, e.g., Ellis [1975], Krausche et al. [1976], Flagg, Krausche and Lebo [1976], Riihimaa [1977]). However, in the model discussion that follows, only the simple-burst morphology described above and illustrated in Figure 7.12 is considered.

A major clue in the attempt to understand *S* bursts came with the discovery that the drift rates were frequency dependent, increasing in absolute value nearly monotonically with frequency between about 5 and 20 MHz. Ellis [1974] showed that electron cyclotron radiation from electrons that conserved the first adiabatic invariant of motion about field lines would drift in frequency with monotonically increasing rates, and that the observations could be matched provided nearly monoenergetic (3-keV) electrons with narrow, that is, conical (3.5° equatorial) pitch angle distributions are assumed. In view of the manifestly Io-related nature of *S* bursts, the initial electron acceleration is assumed to take place at Io in this model. Further, because the drift rates are always negative, it is presumed that the radiation is only observed following reflection of the electrons from their mirror points that are near the top of Jupiter's ionosphere. That is, outward streaming electrons generate negatively drifting emission because of the constantly decreasing field magnitude and hence cyclotron frequency. These, then, are trapped or quasitrapped electrons.

A key feature of this model was the prediction of (1) a turnover in the drift rate vs. frequency curve (near 27 MHz, see Ellis [1974]), and (2) virtually zero drift rate at the

mirror point (i.e., the high frequency cut-off) where the electron velocity parallel to **B** is zero. Thus, the critical test of the model was provided by observations at 32 MHz [Desch, Flagg, and May, 1978]; drift rates, instead of being zero, exceeding any previously recorded at lower frequencies. Subsequent observations at 34 MHz, within a few MHz of the mirror-point frequency (based on the magnetic field model), confirmed this result [Flagg and Desch, 1979]. Because no turnover in the spectrum was seen, this was clearly in conflict with model predictions.

Desch et al. argued that the model was basically sound but that, in order to explain the large drift rates they measured at high frequency, the electron acceleration responsible for the *S* bursts must take place in Jupiter's ionosphere, not at Io. Implicit in this observation was the additional requirement that the initial pitch angles be relatively far removed from 90°. These are decidedly nonmirroring, untrapped electrons. Subsequent observations of a similar nature by Leblanc et al. [1980] and by Ellis [1980] yielded the same conclusions, although Ellis in addition showed that, over the frequency spectrum below 30 MHz the best agreement with observations was obtained with 3 keV electrons possessing a broad range of initial pitch angles at the acceleration point in Jupiter's ionosphere.

At the same time that the high frequency observations were being made, Riihimaa [1979] challenged the evidence that the drift rates were frequency dependent at all. In observations conducted at 22 MHz over many years, he showed that average drift rates could vary widely from storm to storm. The controlling factor in determining drift rates, he contended, was not observing frequency but observer viewing geometry, namely D_E. This particular issue was resolved by Flagg and Desch [1979] who showed that when simultaneous, multifrequency observations are made the frequency dependence is still evident. Thus, there seemed to be a strong short-term dependence on frequency, and for reasons as yet unexplained, a weak long-term (11.9-yr) dependence on D_E.

Narrow-band events (*N* events). A third class of emission events, which are apparently distinct from the *L* and *S* bursts, has been studied in detail by Riihimaa [1968, 1977]. These are the narrow-band events, or *N* events (this designation has not previously been used in the literature), frequently seen in the source B region between 21 and 30 MHz. They have also been observed by Krausche et al. [1976], Flagg, Krausche, and Lebo [1976], Ellis [1979], and Leblanc, Genova and de la Noe [1980]. As mentioned earlier, narrow-band emissions were also observed with relatively low time resolution by Warwick [1963a] and by Dulk [1965] as the extended tails of the spectral landmarks. However, the events observed by Riihimaa do not seem to be part of known spectral landmarks. They have a bandwidth of about 200 kHz and durations anywhere from a few seconds, characteristic of *L* bursts, up to tens of minutes. Bandwidths of *L* bursts are usually about 2 to 5 MHz. An example of an *N* event of at least 9-min duration is shown in Figure 7.20. A question which immediately comes to mind is that if *L* bursts represent what is left over when longer duration bursts are broken up by interplanetary scintillation, how do the *N* events survive being broken up too? Although this question has not yet been answered, Riihimaa's statement that they are among the most intense of Jupiter's bursts may be a clue. Perhaps they are so intense that the scintillation minima are still strong while the maxima saturate the receiving-recording system.

Although the center frequency of an *N* event remains nearly constant, or at most displays a slow but random drift, sometimes it flutters rapidly back and forth between two frequencies. Often a single *N* event flares out into a train of *S* bursts with individual drift ranges much wider than that of the original *N* event.

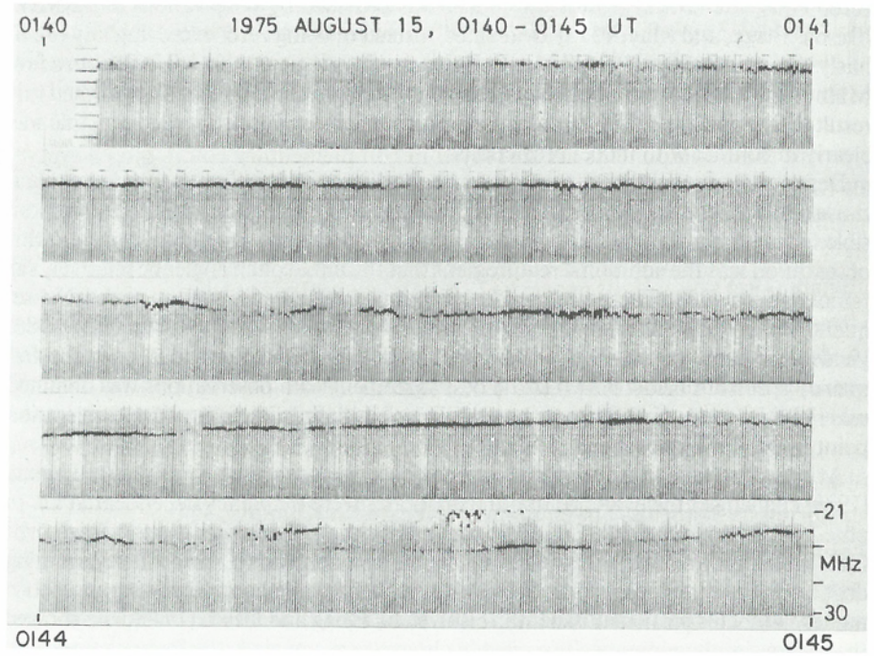

Fig. 7.20. An *N* event is shown starting in the upper left-hand corner and progressing in 1-min sections from left to right and from top to bottom. Five minutes of the original 9-min event are shown. From Riihimaa [1977].

Sometimes interactions occur between an *N* event and *S* bursts that originate well outside the *N* event but drift into it [Riihimaa and Carr, 1981]. In a typical interaction, the drifting *S* burst crosses the *N* event, leaving a "tilted-V-shaped" gap in the latter. The gap represents a quenching of the *N* event for a substantial fraction of a second – far longer than the duration of the *S* burst that triggered it. Much more intricate interaction patterns are produced when the *N* events are fluttering in frequency simultaneously with being cut across by *S* bursts from outside.

Riihimaa [1968] and Boischot et al. [1980] have observed split *N* events, consisting of long enduring parallel pairs of narrow emission bands. They are separated by a sharply delineated narrow band containing no activity. Excellent examples of such events are shown in Figure 7.3 of Riihimaa [1968].

Riihimaa and Carr [1981] consider the possibility of explaining (1) the *S* bursts as arising from bunches of electrons emitting Doppler-shifted cyclotron emission as they ascend a flux tube, (2) the *N* events as gyroemission from a fixed field location by a different population of electrons streaming through it, and (3) the observed interaction as the result of the invasion of the stationary *N*-event emission region by the ascending *S*-burst group. They concluded that it is difficult to explain the more complex interactions by means of such a simple model.

Beaming effects. Evidence for sharp beaming of DAM was provided initially by ground-based observations of the variations in several emission parameters with observer viewing geometry [Douglas, 1964]. Gulkis and Carr [1966] showed, for example, that the centroid of source A varied almost sinusoidally in System III longitude with a period of 11.9 yr, a time interval corresponding to the planet's orbital period. The important parameter that varies over this period is the observer's jovigraphic latitude, or D_E. (The jovigraphic latitude of the Sun, D_S, also varies almost in phase with D_E during this period but the possibility of a D_S dependence has been largely ruled out by the observations that show a slightly better correlation with D_E.) D_E changes by only $\pm 3.3°$ over 11.9 yr; however, the radiation is apparently so strongly beamed in latitude that this excursion is enough to produce the observed results. Changes in occurrence probability with D_E are shown in Figure 7.13. Carr [1972b] showed that both the longitude oscillations and the variations in overall occurrence probability of source A were consistent with a rotating radiation beam having a leading edge parallel to the spin axis and a wedge-shaped trailing edge. The radiation escapes in a direction that favors the northern hemisphere.

Since this early work, additional D_E-dependent phenomena have been found, notably the long-term variations in the Io- controlled source centroids in Io phase [Lecacheux, 1974; Thieman, Smith, and May, 1975] and also in CML [Boyzan and Douglas, 1976]. The effect is strongest for the Io-B and Io-C sources whose oscillations in γ_1 are in phase and of peak-to-peak amplitude 5° to 10°. There is not yet general agreement as to the behavior of Io-A, probably owing to confusion between Io- related and non-Io-related components. Lecacheux [1974] argued that the strong latitudinal beaming implicit in the observed D_E control of the preferred Io phases is inadequately accounted for by the conical sheet model of Dulk [1965] (but see Goldstein and Eviatar [1979]). However, Desch [1978] obtained quantitative agreement with the observations by simply requiring that the emission be radiated from the Io flux tube at a preferred angle to the ambient field regardless of observer vantage point. The results agreed with and lent credence to the source location assignments inferred from polarimetry, namely Io-B in the northern and Io-C in the southern hemisphere.

Estimates of the actual emission beamwidth have been made through examination of dynamic spectra [Warwick, 1963a; Alexander, 1975] and through direct stereoscopic measurement from space [Poquerusse and Lecacheux, 1978]. (However, observations made at the same time by Reyes and May [1981] appeared not to be entirely consistent with the latter result.) Both stereoscopic measurement and examination of dynamic spectra indicate radiation patterns no greater than 10° wide. An independent estimate comes from observations of the 3 to 6 min timescale inherent in the spectral arc emission. If the beam responsible for the arc is carried past the observer at Jupiter's diurnal rate then the indicated beamwidth can be no greater than 2° to 4°. If the beam is carried with Io's motion, the beamwidth is a factor of four smaller.

Emission in the HOM band also exhibits dramatic changes in morphology as a function of observer latitude. These have been modeled by Alexander et al. [1979] in terms of a 10° wide beam centered at a fixed magnetic latitude of $+3°$. These same studies showed that simultaneous observations of radio events by both Voyager spacecraft showed significant decorrelations when observer angular separations exceeded 3°. This latter result is consistent with the 2° to 4° beamwidth inferred from the spectral arc timescales.

Source size, motion, and structure. Both direct and indirect methods have been used to estimate the size of the radiating source of DAM, and both lead to approximately the same upper limit. Very long baseline interferometry (VLBI) yields a direct measure of source size, or an upper limit if the source is unresolved at the longest baselines. Using baselines of over 400 000 wavelengths ($\sim$7000 km) neither Dulk [1970] nor Lynch, Carr, and May [1976] succeeded in resolving sources responsible for either *S* bursts or

L bursts, indicating an angular diameter for these sources of <0.1 arc s, or a source linear dimension of <400 km. One usually assumes that the source is spatially incoherent in deriving this upper bound to the size; however, Ratner [1976] has argued that the limits apply even if the source is spatially coherent.

The other model-dependent estimate of S-burst source size is derived from measurements of the instantaneous bandwidth of the emission. Adopting the model described previously, the instantaneous bandwidth is a consequence of the spatial extent along the Io flux tube (IFT) of an emitting electron bunch. This corresponds to the instantaneous linear physical dimension of the source. Near the surface of Jupiter, the magnetic field gradient in terms of electron cyclotron frequency is about 1 kHz/km, indicating a source size <200 km for bandwidths <200 kHz. This is consistent with the direct VLBI measurements.

VLBI also provides a possible means of detecting source motion in certain directions. Analysis by Lynch, Carr, and May [1976] of the interferometer fringe stability over short time scales (<0.5 s) has shown that the fluctuations in source position parallel to the interferometer baseline is less than 0.05 arc s, or <150 km. They concluded that all the members of a sequence of S bursts, at a given frequency, must come from the same source. A similar investigation of fringe stability by Dulk [1970] led to the conclusion that the L-burst source cannot fluctuate spatially by more than 0.20 arc s.

VLBI has also been used to search for direct evidence of sweeping effects in the radiation beams responsible for S bursts. Based on the simultaneous arrival, within experimental error, of the burst envelopes at two widely-separated stations (after accounting for light travel time), Lynch, Carr, and May were able to rule out the possibility of sweeping beams carried along either with Jupiter's diurnal motion or with Io's orbital motion. They also found no evidence of the beam sweep that would result from a group of radiating electrons moving along a curved magnetic field line. This would seem to contradict the S-burst model described earlier. However, if the electron energy were greater than about 3 keV with near-zero pitch angle (or higher energies with commensurately larger pitch angles), the beam-sweep effect would have been undetectable. Using a refined statistical approach applied to 26 MHz VLBI data, Ratner [1976] came to much the same conclusions regarding the lack of evidence for sweeping-beam effects. All investigators agree that the millisecond-burst structure must result from the emission mechanism itself rather than from the passage of a beam pattern across the observer.

Concluding remarks concerning DAM

In this section we review what is known and what is not well understood about the phenomenology of DAM. The more important of the first-order observational features of DAM that are generally recognized are:

1. The flux density spectrum has a broad peak near 10 MHz and an intrinsic high-frequency cut-off near 39.5 MHz.
2. There is a strong, periodic organization of the activity into storms, with durations of hours, that are modulated on timescales from min to ms. The detailed emission patterns that make up the storms are predictable functions of observing frequency, CML and γ_I.
3. Activity above 20 MHz is predominantly RH elliptically polarized; at lower frequencies either polarization sense is observed depending on CML.
4. Although Io acts to enhance the emission intensity and alter the radius of curvature of the arcs, the basic character of the arcs is principally a function of the CML.

5. The Io-related emission is independent of the solar hour angle of the source, but the Io-independent emission shows diurnal as well as CML control.
6. The strong dependence of the DAM emission on observer latitude is evidence of sharp latitudinal beaming of the radiation.
7. At any given frequency the source size is limited to no more than several hundred km.

Apart from the questions concerning the nature of the processes that give rise to DAM, more properly the subject of Chapter 9, there are a number of observational issues and matters of interpretation of the DAM phenomena that remain unsettled. Some of these questions are long standing, such as the location of the radio sources; others have only recently been raised as a direct consequence of the Voyager observations. We will devote some discussion to the important question of the radio source location and, finally, itemize those questions that should be addressed in the near future regarding the observations.

As stated previously, the observations have long been interpreted to indicate the emission takes place at or near the local electron cyclotron frequency [e.g., Warwick, 1970] and, for the Io-related sources at least, on the IFT. If one accepts these conclusions, then only the source magnetic hemisphere is left unspecified, and here a variety of observations have yielded self-consistent answers in all cases except one. For example, few would argue with the conclusion that the Io-B and Io-A sources are in the northern hemisphere. Their peak frequencies, 39.5 and 38 MHz, respectively, are attainable only in the northern hemisphere. The predominant polarization is RH, consistent with extraordinary-mode emission from Jupiter's northern hemisphere. And the measured long-term oscillation of Io-B in γ_I is in quantitative agreement with a northern-IFT source. The dynamic spectra of the non-Io counterparts of these two sources have great arcs which are of essentially the same shape, occur at the same longitude and display the same polarization. In addition, both have peak frequencies as great or nearly as great as their Io-dependent complements. Non-Io-A, in addition, has been modeled with some success in terms of a northward-tipped beam. All of these similarities imply the same hemisphere is active for the non-Io-A and B sources as for the Io-related sources.

There is also probably widespread agreement concerning the Io-D source. Io-D emission has characteristics which are in agreement with a southern-hemisphere origin: LH polarization and a modest peak frequency of 18 to 20 MHz.

The Io-C source presents some difficulties, however. Both LH and RH polarizations are evident, with the former often dominant below 20 or 22 MHz. Barring unknown propagation effects, extraordinary-mode emission requires that the LH polarized emission originate in the southern hemisphere, where the wave vector is initially antiparallel to $\boldsymbol{B}$. This source exhibits a peak frequency generally not in excess of 30 to 32 MHz, nearly consistent with either north or south, but on some occasions events reach as high as 36 MHz, a fact probably only consistent with a northern hemisphere origin. The 11.9-yr oscillation of the source in γ_I (measured at 22 MHz) is consistent with a southern hemisphere source only, however. Similar comments apply to the non-Io component of the C source, except that the peak frequency has never been observed to exceed 32 MHz, which is probably in the range of frequencies attainable in the southern hemisphere. It is likely that the final answer to the question of source location will have to await direct measurement by ground-based interferometry, if this proves feasible.

Some other points to be settled from either ground-based or Voyager observations are:

1. Is there a distinct component of HOM in addition to the low-frequency extension of DAM? A fraction of the emission below 2 MHz is undoubtedly the extension of greater and lesser arcs into the HOM band. Some of it, however, may represent an independent component.
2. How are the arcs produced? Several theories (see e.g., Chapt. 9) have been advanced to explain arcs; the data must be examined in ways that provide definitive constraints for the various models.
3. What is the relationship between greater and lesser arcs? Unlike much of the greater-arc emission, the lesser-arc emission appears to be more nearly continuous and to be entirely independent of Io control. This suggests an independent origin.
4. How and where do the modulation lanes originate?
5. What aspects of the emission mechanism account for the pronounced differences between *L* bursts, *S* bursts, and *N* events. The observed interactions of *S* bursts with *N* events (and with *L* bursts) are undoubtedly an important new source of information relating to this question, and should provide a stimulus to theoretical activity.
6. Is the interpretation of the *S*-burst observations correct in indicating a source of keV electrons accelerated outward from Jupiter's ionosphere? Most theories provide solely for Jupiterward, that is, Io-accelerated electrons (see, however, Sharp et al. [1978] and Smith and Goertz [1978]).
7. Which interplanetary solar parameter best correlates with the occurrence of non-Io DAM? The weight of evidence now seems to favor the existence of some solar control over the non-Io component of the emission, but the nature of the interaction is unclear. Comparison of in situ measurements by Voyager of solar-wind and interplanetary magnetic field quantities with the occurrence of DAM will be helpful.

7.4. Emissions at kilometric wavelengths

The first evidence for a kilometer-wavelength component of Jupiter's radio spectrum appeared in the Voyager Planetary Radio Astronomy data in April, 1978, when the spacecraft were still more than 2 AU away from their epochal encounters with the planet. By the end of 1978, distinct episodes of LH polarized emissions were routinely being detected at frequencies between 60 kHz and a few hundred kHz. Activity at even lower frequencies in the range covered by the Plasma Wave Science instrument also became commonplace. Such events would be nearly impossible to detect from a spacecraft near Earth because of the overwhelming presence of intense terrestrial kilometric radiation. However, for an observer situated well away from Earth, the Jovian kilometric emissions are often readily recognized by virtue of their distinctive dynamic spectral characteristics, their high degree of polarization, and their tendency to occur at CML values between 120° and 270° where HOM activity is rare.

The first brief reports of the new low frequency emissions appeared in the initial accounts of the Voyager 1 and 2 Jupiter encounters [Scarf, Gurnett, and Kurth, 1979; Warwick et al., 1979a,b; Gurnett, Kurth, and Scarf, 1979a]. More detailed discussions have been given by Kurth et al. [1979a, 1980] who described spectral, spatial, and temporal characteristics observed between about 10 and 56 kHz and by Desch and Kaiser [1980] who studied the occurrence patterns, polarization, and intensity spectra for the frequency range between 20 kHz and about 1 MHz. Green and Gurnett [1980] used a ray-tracing calculation to model the refraction of the kilometric waves in the Io plasma torus to demonstrate that the source region is probably located on auroral field

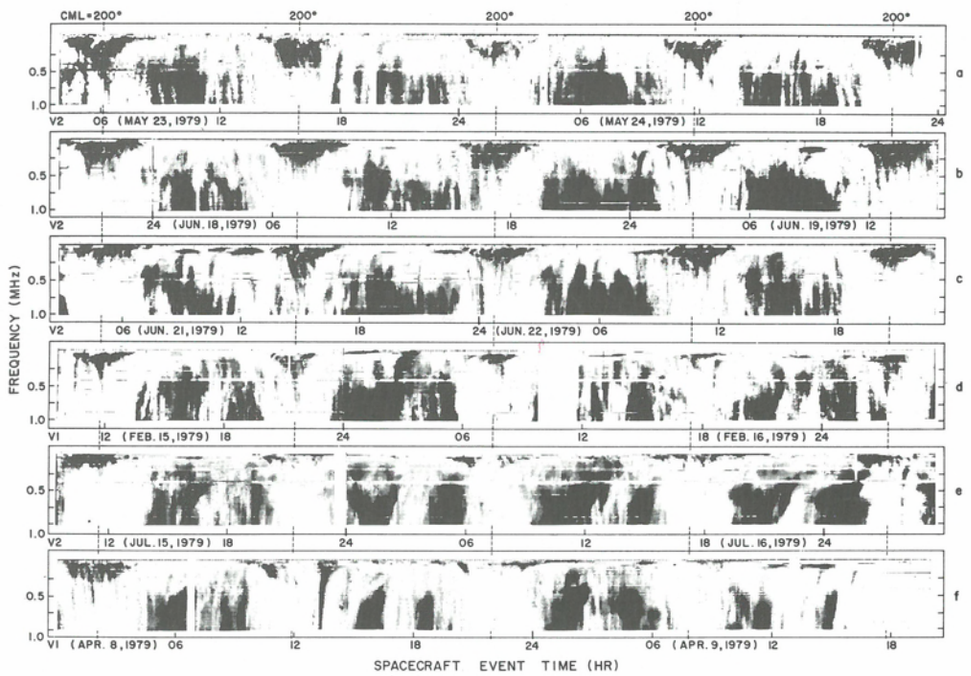

Fig. 7.21. Examples of dynamic spectra of HOM and KOM emissions. Each panel is a frequency-time display of signal intensity recorded between 20 kHz and 1.0 MHz over an interval of nearly two days, and all are aligned in System III Central Meridian Longitude (CML). The bKOM is usually seen at frequencies below about 0.5 MHz when the CML is near 200°. The higher frequency emission that occurs outside the longitude band 200° ± 90° is the HOM. The top four panels are examples of preencounter, dayside obervations of Voyager 2 (*a*)–(*c*) and Voyager 1 (*d*). The two bottom panels are examples of post-encounter, nightside observations from Voyager 2 (*e*) and Voyager 1 (*f*). Examples of nKOM can be seen in between the bKOM events in panels (*c*) and (*d*).

lines between the Io torus and the Jovian ionosphere. Desch and Kaiser [1980] further suggested that the source appears to be fixed in local time rather than to rotate with the planet. Thus the 10-h periodicity was attributed to variations in the observer's magnetic latitude.

Some investigators have referred to the kilometer-wave emissions as "Jovian kilometric radiation" in analogy to the "terrestrial kilometric radiation" or "TKR" first discussed by Gurnett [1974]. We adopt the convention initiated by the Voyager planetary radio astronomy investigators in which the Jovian kilometric radiation is denoted KOM in order to distinguish it from its higher frequency spectral cousins DAM, DIM, etc. As we have noted early in this chapter, there are two apparently distinct kilometric emissions – the broad-band kilometric radiation (bKOM) and the narrow-band kilometric radiation (nKOM) – and we will discuss them below in that order.

Broadband kilometric radiation

Several representative examples of dynamic spectra of individual bKOM events are shown in Figure 7.21. In each case we see a period of emission extending over an hour or more and covering a frequency range of several hundred kHz. The events tend to

last longer at low frequencies than at high frequencies. The dynamic spectra also show evidence of slow drifts in frequency on a scale of ~10 min, and we shall return to these later. Notice also that both the high frequency and low frequency limits to the emission vary from event to event. For example, the first bKOM event in Figure 7.21*c* (~05 hr on June 21, 1979) extends in frequency only up to about 300 kHz, but in the next event 10 hr later we see emission reaching up to at least 800 kHz. Similarly, in the events displayed in the top panel (Fig. 7.21*a*) we see low frequency cut-offs that range from ≤20 kHz to about 100 kHz. The examples in Fig. 7.21 are ordered according to the jovigraphic latitude and local time of the observing spacecraft. The events in Figure 7.21*a–c* were obtained by Voyager 2 prior to closest approach from a jovigraphic latitude of +7° and a local time meridian of 9.5 hr. The events in Figure 7.21*d* were obtained with Voyager 1 from a slightly lower latitude (+3°) and from nearly the same dayside local time sector (10.5 hr). The events illustrated in Figure 21e and f were obtained from above the post-midnight local time sector and at a latitude (+5°) that was intermediate to that for the other panels.

The events recorded from above the daytime hemisphere (Fig. 7.21*a–d*) are all similar in the sense that they show a characteristic tapered shape in which the higher frequency portions occur only during a limited longitude interval centered on 200° CML. The events recorded by Voyager 2 at the higher latitude tend to extend over a wider longitude range than the Voyager 1 dayside events, and this is typical of most (but not all) bKOM activity observed by the two spacecraft before closest approach. Most of the post-midnight sector examples (Fig. 7.21*e, f*) are distinctly different. The high frequency activity peak near 200° longitude is not observed, and instead we see two periods of emission over a limited frequency range and centered at about 150° and 240° CML. Although there is considerable variability in all aspects of the individual dynamic spectra observed from above the sunlit and nightside hemispheres of Jupiter, the trend illustrated in Figure 7.21 is typical of most of the Voyager data. Namely, bKOM events tend to build toward a maximum at 200° CML when observed from the morning sector and to display a "bite" in the dynamic spectrum at 200° CML when observed from above the post-midnight sector.

The drifting structure seen in the individual dynamic spectra is a common feature of bKOM. Both positively and negatively drifting features can occur – sometimes simultaneously – although both Kurth et al. [1979a] and Warwick et al. [1979b] reported that negatively drifting structures appeared to be prevalent in events observed before encounter. Subsequent studies have shown the reverse to be true after encounter. The drift rates are generally greater at high frequencies than at low frequencies and are typically ~1–10 kHz/min at 100 kHz and below.

If the frequency drifts are related to the motion of an exciter along a gradient in the density or magnetic field in the source region then the overlapping occurrence of features of opposite senses of drift must imply the simultaneous occurrence of "ascending" and "descending" sources. The measured drift rates correspond to significantly lower velocities than would be expected for either energetic particles or Alfvén waves in any region between Io's orbit and the Jovian ionosphere. Thus, the drifting bKOM features are not easily explained by simple analogy to drifting solar radio bursts. Both the typical durations of the drifting bKOM features at a single frequency and their frequency-time slopes are roughly comparable to the durations and slopes of the DAM arcs at low frequencies. However, no evidence has been presented to date to demonstrate any physical connection between the two phenomena.

On the shortest timescale at which the bKOM activity has been studied (~60 ms) the emission is found to be very impulsive. An example of this property of the bKOM events is shown in Figure 7.22 where we can see large amplitude fluctuations in measurements taken every 6 s. Kurth et al. [1979a] found that in the frequency range between about 5 and 12 kHz the short, impulsive bursts appeared to be superposed on a relatively smooth background. Moreover, the short bursts drifted systematically at rates of the same order of magnitude as the drift rates for the longer duration features evident in Figure 7.21.

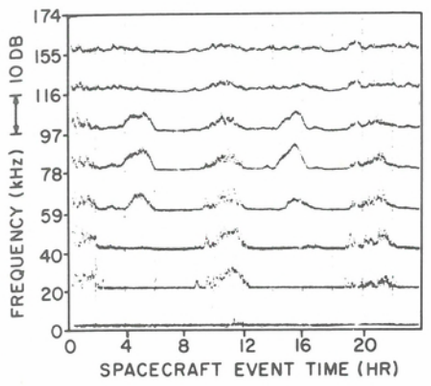

Fig. 7.22. Plots of relative signal intensity at eight frequencies between 20 and 174 kHz as measured by Voyager 2 on May 27, 1979. bKOM events occur at approximately 01, 11, and 21 h spacecraft event time and nKOM events can be seen between 78 and 116 kHz at about 05 and 15 h. Notice that when examined with 6-s time resolution the bKOM is bursty and nKOM is relatively smooth. Adapted from Boischot et al. [1981].

Scarf et al. [1979] noted that bKOM could often be detected down to a minimum frequency between 5 and 10 kHz. Because such a low frequency cut-off is still significantly above the cut-off frequency for electromagnetic waves propagating in the solar wind in the outer solar system, the bKOM low frequency cut-off must be imposed near Jupiter. Scarf et al. suggested that the electron plasma frequency of the Jovian magnetosheath (typically ~5 kHz) could determine the lowest frequency at which an observer outside the Jovian magnetosphere can detect bKOM. On many occasions the low frequency cut-off is greater than 20 kHz (see discussion of Fig. 7.23), and Warwick et al. [1979b] reported that the cut-off frequency extent of the bKOM was probably set by propagation through the Io plasma torus.

Representative power flux densities of bKOM emissions are shown in Figure 7.23. The data are taken from the statistical analysis of 12-day spans of Voyager observations by Desch and Kaiser [1980]. The two solid curves display the most commonly occurring flux density as a function of frequency (mode spectrum) and the flux density that was exceeded only 10% of the time at each frequency (peak spectrum) as observed by Voyager 2 before Jupiter encounter. Only periods of time when the bKOM source was active were included. Spectra of individual events can vary considerably, both within the event and from event to event, but the curves in Figure 7.23 provide a good statistical summary of the average bKOM spectrum. The greatest flux density occurs most often between 60 and 80 kHz, and the half power bandwidth is approximately equal to the frequency at the peak. Only about 10% of the events are observed to extend below 20 kHz or above 1 MHz.

The dashed curve in Figure 7.23 shows the mode spectrum from the post-encounter Voyager 1 data. We see that after encounter the measured flux density levels are generally lower than observed before encounter, the peak frequency is lower, and the emission does not often extend to frequencies as high as are observed in the preencounter data set. Thus the average spectral properties of bKOM resemble the pattern observed for the terrestrial kilometric radiation [Kaiser and Alexander, 1977] where high flux densities and higher frequencies are observed from above one hemisphere and lower flux levels and slightly lower peak frequencies are detected from above the opposite hemisphere. In the case of TKR, the data clearly indicate a source region in the midnight sector that radiates preferentially in directions over the nighttime

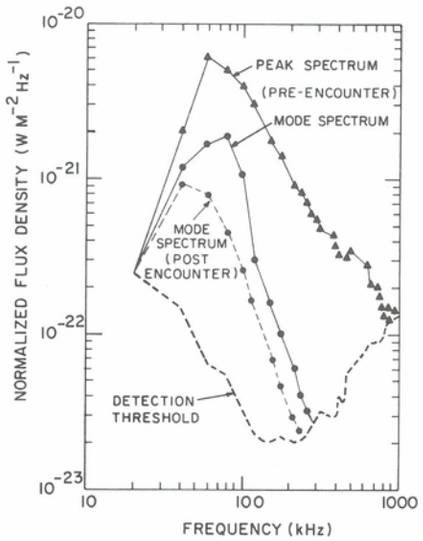

Fig. 7.23. Power flux density spectra of bKOM showing the spectrum most commonly observed before and after Voyager 2 encounter (mode spectrum) and the spectrum representative of the strongest bKOM events (peak spectrum). From Desch and Kaiser [1980].

hemisphere. On the other hand, Desch and Kaiser [1980] argue that the bKOM measurements are most simply explained by a source that favors the daytime hemisphere.

If the radiation is assumed to be emitted uniformly over 4π sr, the isotropic equivalent total radiated power derived by integration of the preencounter mode spectrum is 8×10^8 W. Using a slightly different method, Alexander et al. [1981] find an average power of 3×10^8 W in the kilometric band. The peak power radiated by bKOM as derived from the peak spectrum in Figure 7.23 is 2×10^9 W, and Desch and Kaiser [1980] report that a level of 5×10^9 W is exceeded only 1% of the time. After encounter, the total integrated flux is lower by about a factor of 2.5.

The results of a statistical analysis by Desch and Kaiser [1980] of the variation of occurrence probability of bKOM as a function of CML and Io phase are illustrated in Figure 7.24. The emissions are tightly confined in CML, but the two-dimensional time-line plots give no indication for any dependence on Io phase. The histograms show the variation of 97 kHz activity with CML for three different time intervals. The two preencounter histograms have a single longitude maximum centered between about 190° and 240°, but after encounter when the Voyager 1 spacecraft was above the post-midnight local time sector the CML histogram shows a bimodal distribution with peaks near 150° and 240°. The Voyager 2 data, not displayed in Figure 7.23, also showed a similar split in the post-encounter CML profile. Thus, on a statistical basis, one finds a pattern in the occurrence of bKOM that is typified by the individual events illustrated in Figure 7.21. In particular, the shape of the longitude distribution of bKOM depends on the observer–Jupiter–Sun angle.

In addition to changes in the shape of the CML profile of occurrence probability, the absolute levels of activity appear to depend on observer–Jupiter geometry. Desch and Kaiser [1980] noted that at 97 kHz both the peak occurrence probability and the average occurrence probability over the 120°–270° CML sector of bKOM activity were significantly higher for the Voyager 2 preencounter data than for the other data sets illustrated in Figure 7.24. This seems to be primarily a consequence of the higher jovigraphic latitude at which the dayside Voyager 2 data were collected. Gurnett et al. [1979] also noted that at frequencies between 10 and 56 kHz the bKOM was clearly

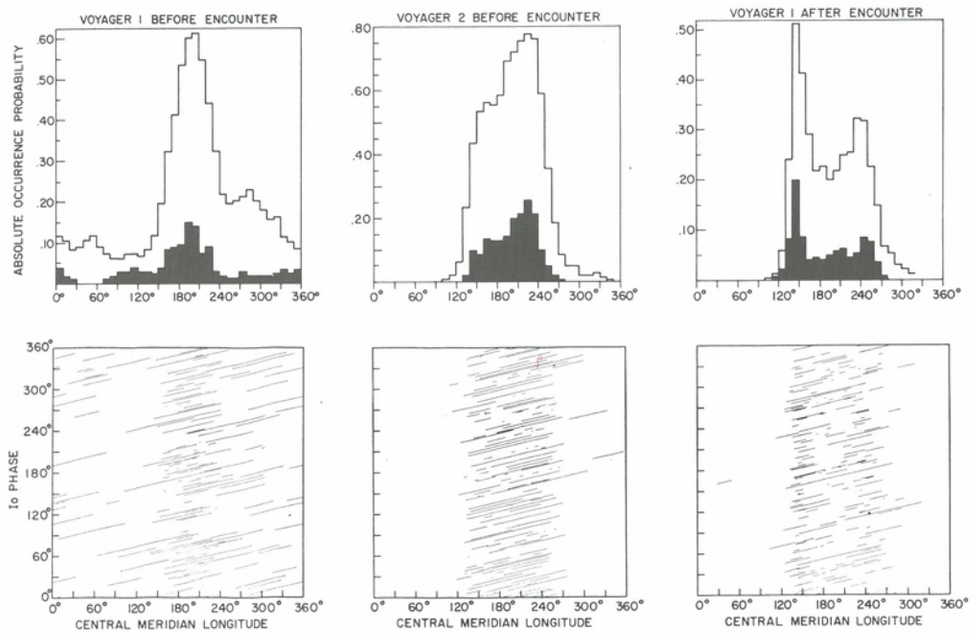

Fig. 7.24. Plots of the occurrence of bKOM at 97 kHz as a function of Central Meridian Longitude (upper panels) and as a joint function of longitude and Io phase (lower panels). The unshaded (shaded) histograms include only those events exceeding a normalized flux density of 2.5×10^{-22} (2.5×10^{-21}) W/m^2/Hz. The activity does not appear to be as tightly organized in longitude in the Voyager 1 preencounter plot because the distinct nKOM events were not purged from the data set. Notice (1) the bifurcation of the longitude peak after encounter and (2) the lack of evidence for any influence by Io. Adapted from Desch and Kaiser [1980].

more intense and more regular in the higher latitude Voyager 2 preencounter data than in the Voyager 1 preencounter data set. Kurth, Gurnett, and Scarf [1980] suggested that at 56 kHz there is a shadow zone of half-width $\sim 10°$ centered on the magnetic equator due to refraction by the Io plasma torus. Thus the Voyager 2 preencounter observations from a latitude of $+7°$ (versus $+3°$ for Voyager 1 before encounter) would place the observer farther outside of the shadow zone for a greater period of time during each rotation of the planet. Arguments favoring a low latitude shadow zone were also made by Warwick et al. [1979b] on the basis of Voyager 2 near encounter data and by Green and Gurnett [1980] on the basis of a ray tracing model.

On the other hand, variations in shadowing due to the periodic rocking of the Io plasma torus can not readily explain the bifurcation of the CML histograms in the post-encounter Voyager data. In spite of the fact that the Voyager post-encounter latitude is intermediate to the two preencounter cases in Figure 7.24, Desch and Kaiser [1980] found a slightly lower absolute occurrence probability in their post-encounter survey than in the Voyager 1 preencounter data set. Thus, the level of activity appears to be diminished when viewed from the nightside of Jupiter in addition to being positively correlated with observer's latitude. Such a local time dependence in the occurrence probabilities is consistent with the preencounter/post-encounter differences in flux densities illustrated in Figure 7.23.

In addition to the major concentration of bKOM activity that occurs near CML = 200° when the northern tip of Jupiter's magnetic dipole is tilted toward the observer,

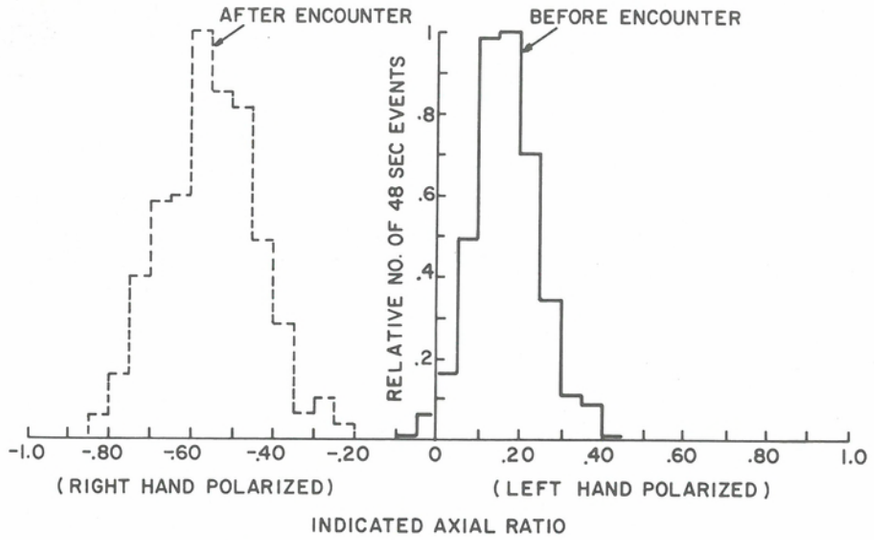

Fig. 7.25. Histograms of the polarization axial ratio of bKOM at 97 kHz as measured simultaneously from above Jupiter's day hemisphere by Voyager 2 (solid lines) and from the night hemisphere by Voyager 1 (dashed lines). Notice that the polarization is almost exclusively left-hand in the first case and right-hand in the latter. Adapted from Desch and Kaiser [1980].

both Scarf et al. [1979] and Warwick et al. [1979a] noted that there exists a subsidiary concentration of emission at longitudes between about 20° and 40° or in roughly the longitude range of the Southern dipole tip. This component is considerably weaker and more intermittent than the emission near 200°. In contrast to the positive latitude correlation in the 200° bKOM activity, the bKOM events at early longitudes were more common in the Voyager 1 inbound data than in the corresponding Voyager 2. This inverse correlation with observer's latitude lends support to the physical association of the 200° emission with a northern hemisphere source and the 20°–40° emission with a southern source.

The polarization properties of bKOM are particularly interesting. By examining the long-term statistical behavior of the bKOM polarization and by interpreting the results as time-averaged properties, Desch and Kaiser [1980] were able to specify more than just the polarization sense of the waves. They found that the emission appears to be strongly polarized over essentially its full frequency range (~20 kHz to 1 MHz). The degree of polarization must be at least 75% and could be as high as 100% polarized. Statistical studies of the measured wave axial ratio also suggest that the waves must be more nearly circular rather than linearly polarized.

Desch and Kaiser [1980] also reported that the sense of polarization of bKOM reverses depending on whether the observer is situated over the dayside or the nightside of Jupiter. When viewed from above the day hemisphere, bKOM is LH polarized; when viewed from above the night hemisphere, the polarization is RH. This remarkable result is illustrated in Figure 7.25, which shows histograms of indicated axial ratio at 97 kHz observed by Voyager 1 and Voyager 2 at the same time but from two different local time locations. Voyager 1 was in the post-midnight sector after encounter and measured the bKOM to be exclusively RH. During the same period of time Voyager 2 was approaching Jupiter from above the prenoon sector and detected bKOM that was

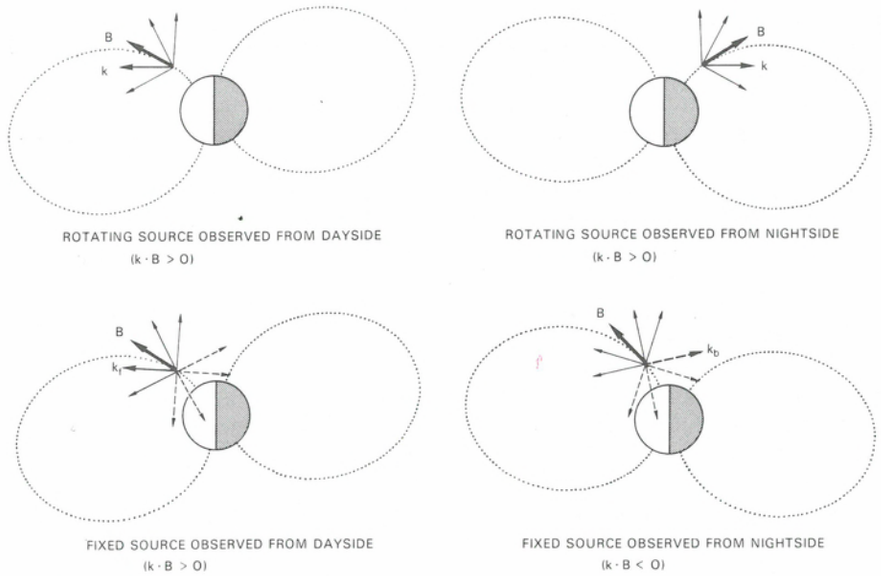

Fig. 7.26. A schematic illustration of some differences between a rotating, light-house-like radio source (upper panels) and a source that remains fixed in local time and emits into a forward (f) and back (b) lobe (lower panels). The source rotating with the planet would always appear to have the same polarization sense, because the relative orientation of the magnetic field B and the wave vector **k** would always be the same with respect to the observer. For a fixed source, the forward lobe wave vector $\mathbf{k}_f$ and the backward lobe wave vector $\mathbf{k}_b$ are reversed with respect to B. Hence a viewer on the nightside would measure the opposite polarization compared to a dayside observer if the source remains near a particular local time meridian.

predominantly LH polarized. Both spacecraft observed the polarization reversal with respect to the time of passage from the sunward hemisphere to the nightside hemisphere at encounter. Although very little information exists on the polarization of the secondary component of bKOM observed at longitudes around 20°–40°, Desch and Kaiser [1980] report that just before Voyager 2 encounter, when the 200° emission was LH polarized, activity at the earlier longitudes was clearly RH.

Desch and Kaiser [1980] argued that the polarization data are strongly suggestive of a radio source that remains fixed in some local time zone rather than one that rotates around the planet. The base mode for a particular electromagnetic wave, ordinary or extraordinary (O or X), will have a particular sense of polarization that will depend on whether the wave normal vector, **k**, has a component that is parallel or antiparallel to the magnetic field vector, **B**, at the source. A source that is constrained to a fixed range of longitudes and that rotates around the planet in synchronism with the rotation of the magnetic field will always have **k** oriented in the same sense with respect to **B** when observed at the same CML regardless of the observer's local time. However, for a source that does not rotate with the planet an observer above the sunlit hemisphere would detect emission of one polarization, and an observer above the opposite hemisphere would detect the opposite polarization because the waves escaping in the two opposite directions would have **k** in the opposite sense with respect to **B**.

This situation is illustrated in Figure 7.26. For a northern hemisphere source located near the planet (as opposed to near the Io plasma torus), a "forward lobe" will have a

wave vector component $\mathbf{k}_f$ parallel to **B**, and a "back lobe" of the same source will have a wave vector component $\mathbf{k}_b$ antiparallel to **B**. Thus the two lobes will be seen to have opposite polarizations. If the observed polarization is unchanged when viewed from both day and night hemispheres, then we always observe forward lobe radiation. For the polarization to reverse, we must be seeing foward lobe radiation when above one hemisphere but back lobe radiation when above the opposite hemisphere. Absorption or refraction effects associated with the propagation of back lobe waves over the polar cap toward the night hemisphere are likely to contribute to the lower intensity and occurrence probability observed for the nightside data.

The data do suggest a northern hemisphere source for CML $\sim 200°$ because the profiles of occurrence probability show a direct correlation with latitude. The maximum in the histograms produced by both Desch and Kaiser [1980] and Kurth et al. [1979a, 1980] occur when the observer's magnetic latitude reaches its greatest northern value. This corresponds to the greatest amount of tipping of an obscuring Io plasma torus out of the way of the line of sight to a source in the northern hemisphere. Furthermore, the higher flux densities and occurrence probabilities observed in the preencounter dayside data sets suggest a source located in the day hemisphere.

If we accept the evidence for a northern hemisphere, dayside source as sketched in Figure 7.26, then we can also infer the electromagnetic wave mode. Because we observe LH polarization for the forward lobe when **k** is parallel to **B** in the north, the radiation must be in the ordinary mode. Green and Gurnett [1980] also noted that if the bKOM is associated with the Io plasma torus or with magnetic field lines that thread the torus, then a comparison of the low frequency limit of bKOM with the range of propagation cutoffs inside $\sim 10\ R_J$ implies left-hand ordinary (L-O) rather than right-hand extraordinary (R-X) mode emission. They pointed out that since bKOM is observed to frequencies as low as 10 kHz, the propagation cut-off frequency at the source must be below 10 kHz. Because the R-X cut-off is determined by the upper hybrid frequency, which is greater than about 50 kHz everywhere inside the likely source region, the R-X mode can be ruled out.

The bKOM is sporadic on a timescale of hours and longer. Successive individual events do not necessarily occur at the same flux density levels or with identical dynamic spectral shapes. Both the high frequency and the low frequency cut-offs can change by a factor of ~ 3 in just a few rotations of Jupiter, and the emission can occasionally disappear entirely for several rotations. Kurth et al. [1980] developed a simple bKOM activity index based on the total intensity observed at 56 kHz over one rotation of Jupiter. When plotted as a function of time, this activity index exhibited marked fluctuations on a timescale of ~ 1–15 days. Kurth et al. [1980] pointed out that these time variations could be indicative of changes in the properties of the Io plasma torus, the injection of fresh torus ions from Io, the interaction of the solar wind with Jupiter's magnetosphere, or some other dynamic process analogous to terrestrial magnetospheric substorms. The analysis of these long term fluctuations in bKOM activity is just beginning to be used as a remote diagnostic of temporal variations in Jupiter's magnetosphere.

Narrow band kilometric radiation

A second, quite distinctive component of Jupiter's kilometer wavelength emissions is the narrow band KOM, or nKOM. This class of emission was first noted in the initial report of Voyager 2 Jupiter encounter results [Warwick et al., 1979b]. Most of the information in the discussion below is taken from the subsequent definitive study of nKOM by Kaiser and Desch [1980].

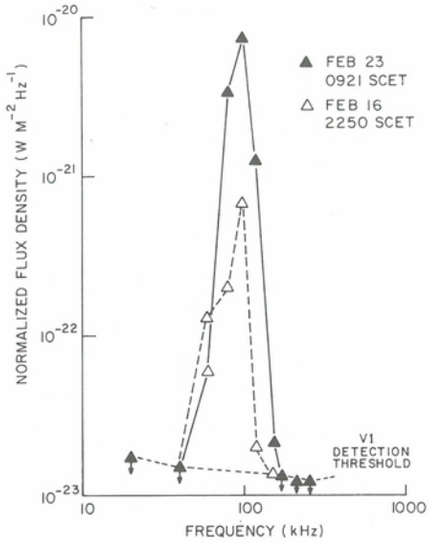

Fig. 7.27. Typical power flux density spectra of nKOM. From Kaiser and Desch [1980].

An example of the dynamic spectral appearance of nKOM can be found in Figure 7.21*c* (0900-1300, 2100-2300 on June 21) and Fig. 7.21*d* (0000-0200 on February 16). The emission occurs at frequencies between about 50 and 180 kHz in events that typically last for a few hours or less. Individual events tend to be composed of a smooth rise and fall in signal level with little or no burstiness noticeable of the sort that is characteristic of the bKOM.

The remarkably narrow instantaneous bandwidth observed for nKOM is illustrated in Figure 7.27. The figure, taken from the report by Kaiser and Desch [1980], shows two examples of power flux density spectra. In each case, we see a peak at about 100 kHz and a very sharp cut-off at both high and low frequencies. Bandwidths of only 40 to 80 kHz are commonly observed. According to Kaiser and Desch, the isotropic equivalent total radiated power in nKOM can occasionally reach $\sim 10^9$ W but is more typically $\sim 10^8$ W.

Polarization measurements of nKOM show that the emission is usually observed to be LH when the observer is situated north of the magnetic equator and is RH when observed from above the southern magnetic hemisphere. Kaiser and Desch [1980] noted that polarization reversals sometimes occur during the course of an individual nKOM event at the time of Voyager spacecraft crossings of the magnetospheric current sheet, but that this was not an invariant property of nKOM.

Initial studies of the Central Meridian Longitude distribution of nKOM were inconclusive because CML histograms of occurrence probability calculated from nKOM event catalogs showed no organized pattern. (In fact, most of the CML-independent activity that appears in the left-hand panel of Figure 7.24 is due to nKOM.) This was considered highly unusual because virtually every other component of the Jovian emission exhibits at least some organization in CML. This puzzle was solved when Kaiser and Desch [1980] plotted the longitudes where nKOM was observed on a rotation-by-rotation basis, and their results are shown in Figure 7.28. We see that the emission tends to occur at slightly later longitudes on each successive rotation of the planet, and the amount of slippage is about the same from one rotation to the next. In other words, the nKOM events do tend to recur periodically but at a rate that is slightly slower than the rotation rate of the planetary magnetic field.

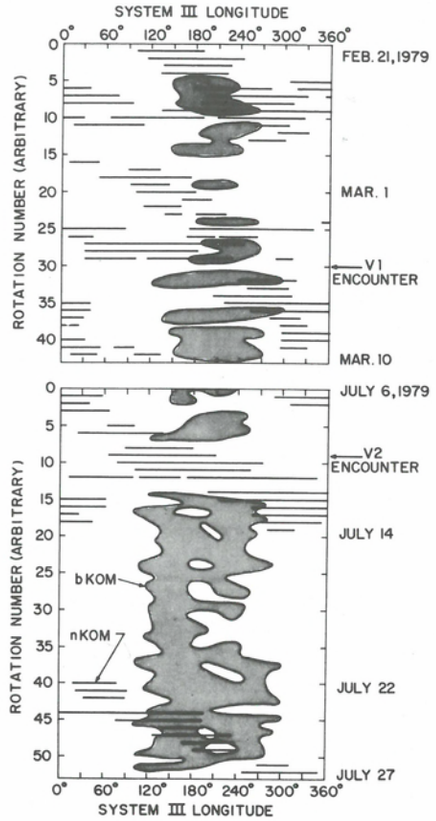

Fig. 7.28. Plots of the occurrence of bKOM (shaded patches) and nKOM (line segments) as a function of date and central meridian longitude. The data are displayed on a Jupiter rotation-by-rotation basis and time, as measured by the number of 10-hr planetary rotations, increases downward. Voyager 1 observations are shown in the top panel and Voyager 2 observations are displayed below. Notice that the bKOM always appears in the longitude band between about 120° and 280° but that nKOM drifts in System III longitude due to its slower recurrence period. Adapted from Boischot et al. [1981].

Kaiser and Desch [1980] found that the best-fit recurrence period for the nKOM activity corresponds to a rate that is 3% to 5% slower than what would be expected for a rigidly corotating source. Based on Hill's [1980] model of the radial breakdown in magnetospheric corotation (see also Chap. 10) this amount of corotation lag would correspond to a source at a radial distance of 8 to 9 R_J, and Bagenal and Sullivan [1981] did observe evidence for 5% to 10% deviations from corotation in plasma ion data taken near the outer edge of the torus. This distance range corresponds to the outer periphery of the Io plasma torus where measured upper hybrid resonance frequency and plasma frequency of the torus electron plasma are essentially identical to the observed nKOM emission frequency, ~100 kHz [Birmingham et al., 1981]. Thus, the outer portions of the torus where departures from corotation are beginning to become measurable are plausible nKOM source locations.

The Voyager data near the times of closest approach provide additional evidence for a source location near or just inside of 10 R_J. Kaiser and Desch [1980] noted that nKOM events were detected before and after Voyager 1 closest approach when the spacecraft was at a radial distance of ~12 R_J and also near the time of Voyager 2 closest approach at 10 R_J. They pointed out that when an observer is situated that close to the Io torus, whose vertical dimensions are $\sim \pm 1$ R_J, refraction makes impossible the detection of a 100 kHz source planetward of the torus. They noted further that there was no evidence in the Voyager data to suggest that the source was situated farther from Jupiter than 10 to 12 R_J, and that the range of electron cyclotron frequencies and

plasma frequencies extant in the magnetosphere beyond this distance are too low to support emission above ~50 kHz. Thus there are at least four lines of evidence for an nKOM source near the outer portion of the Io torus:

1. the detection of a 3% to 5% departure from corotation,
2. the limited range of directions visible during events detected near Voyager closest approach,
3. the unique coincidence of torus electron plasma frequencies and nKOM emission frequencies, and
4. the existence of strong upper hybrid resonance emissions in that region of space that might be the source of the nKOM.

The records of the occurrence of nKOM plotted in Figure 7.28 show that emission is not always observed on every rotation, but instead nKOM is intermittent on a scale of several days. Moreover, a source can disappear altogether and then reappear many rotations later still in phase with its predecessor. For example, in the Voyager 2 plot, emission was observed from a source that drifted across the full 360° range of System III longitudes between about July 6 and July 14, 1979, and then no nKOM was detected during the next 20 rotations of Jupiter. When nKOM emissions appeared again on July 22, they occurred at the same longitude as would be expected if the activity observed prior to July 14 had continued at the same repetition rate.

Two source regions appear to be active in the Voyager 1 plot in Figure 7.28. One region is observed at longitudes from about 100°–190° on February 21, 1979, which then drifts to about 300° CML after a dozen rotations. This region then ceases to be active except for a few rotations just before the time of Voyager 1 encounter when it appears at longitudes between ~ 30° and 180° still in phase with the earlier activity. A second source begins at about 360° CML on February 23 and drifts through a full 360° range of longitudes over the remaining 40 rotations displayed in the plot. Although there are occasional interruptions in activity for a day or so, there is no apparent change in its location or longitude extent even though Voyager 1's closest approach occurred in the middle of the observing span.

Thus, we are presented with a picture of an nKOM source whose physical extent or radiation pattern near the ecliptic plane are confined to a limited longitude range. It rotates at a rate slightly slower than the planetary magnetic field and maintains its identity over long periods of time even though the radio-wave activity visible from near the ecliptic varies episodically, either waxing or waning for days at a time. The emission may be similar to that responsible for terrestrial nonthermal continuum radiation in which narrow-band electromagnetic waves are generated via coupling with electrostatic waves near the upper hybrid frequency [Jones, 1980; Kurth, Gurnett, and Anderson, 1981].

7.5. Concluding remarks

We conclude this discussion of the kilometer-wave radio emissions from Jupiter with a recapitulation of what we believe we know and what we view as the outstanding questions concerning KOM at present (1981).

For bKOM, we know:

1. dynamic spectra, power flux density spectra and occurrence probability profiles as a function of CML all show evidence of a dependence on observer–Jupiter–Sun angle and on observer's latitude;

2. emissions near 200° CML are from a northern-hemisphere source and are LH polarized when viewed from above the sunlit hemisphere but are RH polarized when viewed from above Jupiter's nightside;
3. there exists a complementary southern hemisphere source near CML ~20° for an observer at southern jovigraphic latitudes;
4. a model of the northern-hemisphere source that emits in the left-hand-ordinary mode from a region above Jupiter's dayside ionosphere in the northern hemisphere is consistent with all the observations; and
5. refraction of bKOM waves as they propagate through or over the Io plasma torus is likely to influence the spectral properties observed for bKOM.

For bKOM, we do not yet know:

1. how far above 1 MHz the emission can extend;
2. what is the origin of the drifting patterns seen in dynamic spectra;
3. what is the origin of the observed temporal variations in bandwidth and intensity; and most importantly,
4. what is the emission mechanism.

For nKOM, we know:

1. the emission occurs only over a narrow band of frequencies comparable to the electron plasma frequency near the edge of the Io plasma torus;
2. the repetition rate of the emission is slower than the System III rate by an amount comparable to the corotation lag in the outer edge of the Io plasma torus; and
3. the emission is intermittent, being active for days at a time then disappearing for several days and then reappearing without apparently changing its location in the "not-quite-corotating" frame.

For nKOM, we do not yet know:

1. what causes the polarization reversals often seen during an event;
2. what causes the episodic appearance and disappearance of the emission; and fundamentally,
3. what is the emission mechanism.

ACKNOWLEDGMENTS

The authors are grateful to their colleagues, T. J. Birmingham, M. L. Goldstein, S. Gulkis, M. L. Kaiser, and W. S. Kurth, for their very thorough review and constructive comments on earlier versions of this chapter. We thank J. J. Schauble and J. R. Thieman for providing unpublished data for Figures 7.1 and 7.15, respectively. We also thank B. C. Holland, F. H. Hunsaker, and L. A. White for their untiring efforts in producing the original typescript and most of the illustrations. We acknowledge the partial support of NASA through grant NAGW-196.

8

PLASMA WAVES IN THE JOVIAN MAGNETOSPHERE

D. A. Gurnett and F. L. Scarf

The recent Voyager encounters with Jupiter have now provided us with the first comprehensive investigation of plasma waves in the magnetosphere of Jupiter. The most striking feature of the Jovian plasma wave observations is the close similarity to the plasma-wave phenomena observed in the Earth's magnetosphere. Essentially, all major types of plasma waves detected in the Jovian magnetosphere have analogs in the Earth's magnetosphere. These include, for example, electrostatic waves near and upstream of the bow shock, electromagnetic continuum radiation, lightning- generated whistlers, whistler-mode chorus and hiss, electrostatic electron cyclotron and upper hybrid emissions, and broadband electrostatic noise.

8.1. Introduction

Any waves that are influenced by the presence of a plasma are called plasma waves. Because wave-particle interactions in a collisionless plasma produce scattering and thermalization effects somewhat similar to collisions in an ordinary gas, plasma waves are now recognized as being of fundamental importance for understanding the equilibrium state of planetary magnetospheres. In the Earth's magnetosphere, wave-particle interactions are known to be responsible for heating the solar wind at the bow shock, for the diffusion that allows plasma to enter the magnetosphere, and for the pitch-angle scattering that causes the loss of energetic particles trapped in the magnetic field. A large number of different types of waves can occur in planetary magnetospheres. The properties of some of the more important plasma wave modes are summarized in Table 8.1. In general, plasma waves can be classified as either electromagnetic, which have both electric and magnetic fields, or electrostatic, which have no magnetic field. The electromagnetic modes include two free space modes that can escape from the plasma and be detected remotely and several internal modes, such as the whistler mode, that cannot escape from the plasma. Typically, the electromagnetic modes tend to have propagation velocities near the speed of light. The electrostatic modes, on the other hand, tend to have much lower propagation velocities with properties somewhat similar to sound waves in an ordinary gas. At low frequencies, below the ion cyclotron frequency, plasma waves display a fluidlike behavior involving the bulk motion of the entire plasma. Two such modes, called the shear and compressional Alfvén waves, are the principal mechanisms by which all fluid disturbances are propagated through a plasma. For a further review of the types of wave modes that can exist in a plasma, the reader is referred to one of the standard texts on the subject, for example, Stix [1962] or Krall and Trivelpiece [1973].

The recent Voyager encounters with Jupiter now provide us with the first comprehensive investigation of plasma waves in the magnetosphere of Jupiter. The most striking feature of the Jovian plasma-wave observations is the very close similarity to the plasma-wave phenomena observed in the Earth's magnetosphere. Essentially, all of the major types of plasma waves detected in the Jovian magnetosphere have analogs in the Earth's magnetosphere. These include, for example, electrostatic waves near and upstream of the bow shock, electromagnetic continuum radiation, lightning-generated